Computational screening, synthesis and testing of Metal-Organic Frameworks with a bis(thiazole) linker for carbon dioxide capture and its green conversion into cyclic carbonates

Journal:	*Molecular Systems Design & Engineering*
Manuscript ID	ME-ART-05-2019-000062.R1
Article Type:	Paper
Date Submitted by the Author:	30-Jun-2019

Complete List of Authors:	Muller, Philipp; TU Dresden Bucior, Benjamin; Northwestern University, Department of Chemical and Biological Engineering Tuci, Giulia; ICCOM-CNR, Luconi, Lapo; Area della Ricerca CNR, ICCOM-CNR Getzschmann, Juergen; TU Dresden Kaskel, Stefan; Technische Universitat Dresden, Institut fur Anorganische Chemie Snurr, Randall; Northwestern University, Department of Chemical & Biological Engineering Giambastiani, Giuliano; ICCOM-CNR, Rossin, Andrea; CNR, ICCOM DPM,

Design, System, Application

Metal Organic Frameworks (MOFs) are versatile materials with high internal surface area and instrinsic porosity; nowadays, they are widely exploited in CO_2 capture (CCS) and utilization (CCU) technologies. With this application in mind, a new bithiazole ligand has been prepared and fully characterized to be used as linker for MOFs synthesis. The presence of a basic N-donor in the heterocyclic ring may represent an added value in CCS, because of the great affinity of (acidic) carbon dioxide for bases. The most suitable MOF for the desired application containing this ligand was found through a computational crystal construction algorithm, by building *in silico* a dozen MOF options, with assorted edge-transitive crystal topologies. According to the theoretical analysis, the zirconium MOF of cubic topology isostructural with UiO-67 was the optimal candidate. This MOF was then prepared in the laboratory and fully characterized. It showed indeed good performance in CCS, with a CO_2 uptake of 7.5 %wt. at 298 K and 1 bar. Additionally, the same material was exploited for CCU as heterogeneous catalyst in the CO_2 cycloaddition to epoxides under green (solvent- and co-catalyst-free) conditions, achieving 74% conversion of epibromohydrin to its cyclic carbonate at ambient pressure and at T = 393 K. The results outlined here confirm the positive synergy between theory and experiment for the tailored design of MOFs in specific applications.

Computational screening, synthesis and testing of Metal-Organic Frameworks with a bis(thiazole) linker for carbon dioxide capture and its green conversion into cyclic carbonates

Philipp Müller,[a] Benjamin Bucior,[b] Giulia Tuci,[c] Lapo Luconi,[c] Jürgen Getzschmann,[a] Stefan Kaskel,[a]

*Randall Q. Snurr,[b] Giuliano Giambastiani [c,d] and Andrea Rossin [c,]**

[a] Institute of Inorganic Chemistry, Technische Universität Dresden, Bergstraße 66, D-01062 Dresden, Germany

[b] Department of Chemical and Biological Engineering, Northwestern University, 2145 Sheridan Road, Evanston, IL 60208, United States.

[c] Istituto di Chimica dei Composti Organometallici (ICCOM-CNR), Via Madonna del Piano 10, 50019 Sesto Fiorentino, Italy.

[d] Institute of Chemistry and Processes for Energy, Environment and Health (ICPEES), UMR 7515 CNRS-University of Strasbourg (UdS), 25, rue Becquerel, 67087 Strasbourg Cedex 02, France.

Author to whom correspondence should be addressed: a.rossin@iccom.cnr.it.

Abstract. Computational crystal construction algorithms were used to create twelve metal-organic frameworks containing a newly synthesized [2,2'-bithiazole]-5,5'-dicarboxylic acid (H_2TzTz) spacer and assorted transition metal nodes. Among the twelve structures, the zirconium-based MOF of general formula $[Zr_6O_4(OH)_4(TzTz)_6]$ (**1**) was found to be the best candidate for carbon dioxide uptake, as judged from the results of the grand canonical Monte Carlo (GCMC) simulations of CO_2 adsorption isotherms. Guided by the simulation results, **1** was synthesized in the laboratory and thoroughly characterized. **1** is isoreticular to its bis(thiophene) and bis(benzene) (UiO-67) analogues; it crystallizes in the cubic $Pn\bar{3}$ space group with **fcu** topology, and it features octahedral $[Zr_6]$ nodes connected by twelve carboxylate groups from six bridging $TzTz^{2-}$ spacers. It is a predominantly microporous material (micropore volume = 84% of the total pore volume), with a BET area of 840 m^2/g and a maximum CO_2 uptake at ambient pressure of 2.3 mmol/g (10.0 wt.%) or 1.7 mmol/g (7.5 wt.%) at 273 or 298 K, respectively. The CO_2 affinity (isosteric heat of adsorption Q_{st} = 18.7 kJ mol^{-1}; CO_2/N_2 Henry selectivity = 10; CO_2/N_2 IAST selectivity = 8.4) is similar to that of its bis(thiophene) analogue. After partial removal of solvent (activation), **1** was tested as a heterogeneous catalyst in the reaction of CO_2 with epoxides bearing a $-CH_2X$ pendant arm (X = Cl: epichlorohydrin; X = Br: epibromohydrin) to give the corresponding cyclic carbonates at T = 393 K and p_{CO2} = 1 bar under green (solvent- and co-catalyst-free) conditions. A good conversion of 74% and a turnover frequency of 12.3 mmol(cyclic carbonate) · $(mmol_{Zr})^{-1}$ · h^{-1} have been recorded with epibromohydrin as substrate.

Keywords

Metal-organic frameworks (MOFs) – carbon dioxide – porous materials – thiazole ligands – zirconium – carbon capture and sequestration (CCS) – carbon capture and utilization (CCU) – heterogeneous catalysis – grand canonical Monte Carlo – molecular simulation – structure generation

Introduction

The World population is rapidly increasing, and it is using fossil fuels such as coal and natural gas to satisfy its energy demand. This current situation releases large amounts of carbon dioxide into the atmosphere every year. Some of this CO_2 is absorbed by oceans and seas causing a rise in seawater acidity. Some CO_2 is used by plants in photosynthesis to form organic molecules and oxygen. However, about half of the CO_2 remains in the atmosphere as the primary source of greenhouse gas, which further triggers a series of global environmental and energy problems.[1] Carbon capture and storage/sequestration (CCS) is considered a promising strategy to overcome these issues and make a significant impact in environmental protection and sustainable development.[2] CCS technologies based on adsorption by nanoporous adsorbents have recently become popular; metal-organic frameworks (MOFs) belong to this class of materials and have gained great attention in this context.[3] MOFs hold unique advantages, including the tailored control of their pore size and shape along with high surface area,[4] as well as the possibility to include selected functional groups within their linker.[5] A powerful driving force behind the unprecedented expansion in MOF materials is that a desired framework topology platform and chemical recognition sites can be targeted by the judicious selection of metal clusters and organic linkers.

An alternative approach to reduce CO_2 concentration in the atmosphere and to mitigate its environmental effects moves beyond CO_2 sequestration to Carbon Capture and Utilization (CCU), where CO_2 is no longer regarded as a simple waste but as a renewable resource to be harvested and recycled into C-containing products and feedstocks of added value.[6] CO_2 is abundant, non-toxic, and non-flammable. For these reasons, the utilization of CO_2 as a C_1 feedstock to form other products by chemical fixation would benefit from environmental friendliness and stability during handling. However, CO_2 activation is challenging. The high oxidation state of carbon in CO_2 results in elevated thermodynamic stability, and therefore CO_2 utilization requires reaction with high energy substrates like strained small heterocycles (epoxides, oxiranes). Cycloaddition reactions between CO_2 and epoxides are some of the most efficient approaches to convert CO_2 into valuable chemicals.[7] These reactions produce cyclic organic carbonates which are widely used in the pharmaceutical and chemical industries.[8] Cyclic carbonates are valuable

synthetic targets; since their commercialization in the mid-1950s, they have found applications as polar aprotic solvents, electrolytes for lithium-ion batteries, and as intermediates in the manufacture of fine chemicals. Cyclic carbonates are also used as constituents of oils and paints and as raw materials in the synthesis of polycarbonates and polyurethanes, since they can undergo ring-opening polymerization. Many different heterogeneous catalysts have been exploited to promote cyclic carbonates synthesis.

In a combined [CCS+CCU] perspective, MOFs represent excellent candidates to play the role of both sorbent and catalyst.[6] MOF materials bearing basic N/O/S heteroatoms embedded in their linkers show strong interactions with the (acidic) CO_2 molecule, increasing the concentration of CO_2 within the pores where the catalytically active sites are present.[9] The increased overall bond polarization within the linker is highly desired in gas storage applications; in fact, it has been shown (both theoretically[10] and experimentally[11]) that a MOF with increased bond polarity has an improved gas adsorption capacity for those gases with a very small or zero dipole moment (H_2, CH_4, CO_2). Thiazoles are intriguing (N,S) heterocycles. The N atom in the heterocycle can be protonated under acidic conditions (pK_a = 2.5). As a donor towards Lewis acids, it is less basic than pyridine (pK_a = 5.2) but more basic than oxazole (pK_a = 0.8). Given our previous experience in the field of thiazole-based coordination polymers,[12] we have devoted our attention to the development of [CCS+CCU]-suitable MOFs containing this heterocycle, prompted by the idea that the polarity of thiazole C-S or C-N bonds together with the basicity of its N atom may increase the interaction with CO_2 and strengthen the material physisorption capacity.

With this motivation, the new bidentate linker [2,2'-bithiazole]-5,5'-dicarboxylic acid (H_2TzTz, Scheme 1) has been prepared and fully characterized in solution and in the solid state. Subsequently, a suitable MOF material for CO_2 capture containing this linker has been found through a fully computational approach. Twelve hypothetical MOF structures have been generated by combining H_2TzTz with assorted transition metal nodes. Applied to this specific case, the best candidate for CO_2 adsorption [judging from the results of the grand canonical Monte Carlo (GCMC) simulations of CO_2 adsorption isotherms carried out on the twelve MOF structures] was found to be the cubic zirconium-based MOF with general formula $[Zr_6O_4(OH)_4(TzTz)_6]$ (**1**). Following the suggestion coming from the theoretical

input, **1** has been synthesized in a laboratory scale and fully characterized in the solid state. **1** is a microporous MOF that crystallizes in the $Pn\bar{3}$ space group, confirming the structure found by the computational algorithm. The activated material (after solvent removal from the pores) has been tested both as CO_2 adsorbent (CCS) and as a heterogeneous catalyst for the synthesis of cyclic carbonates (CCU) under mild and green conditions, without the use of solvent and co-catalyst.

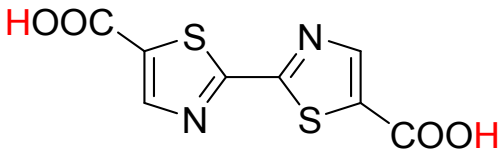

Scheme 1. Molecular structure of [2,2'-bithiazole]-5,5'-dicarboxylic acid (H_2TzTz).

Methods

Materials and Methods. All the commercially available starting materials were of analytical grade. They were purchased from Sigma Aldrich and used as received, without further purification, while the epoxides used in the catalytic tests were distilled prior to use and stored over 4 Å molecular sieves under nitrogen. For the organic syntheses, solvents were purified through standard distillation techniques. Deuterated solvents (Sigma Aldrich) were stored over 4 Å molecular sieves and degassed by three freeze-pump-thaw cycles before use. Diethyl [2,2'-bithiazole]-5,5'-dicarboxylate was prepared according to the literature procedure.[13] X-ray powder diffraction (PXRD) qualitative measurements were carried out with a Panalytical X'PERT PRO powder diffractometer equipped with a diffracted beam Ni filter and an PIXcel© solid state detector in the 4-50° 2θ region, operating with Cu Kα radiation (λ = 1.5418 Å). Anti-scatter slits were used both on the incident (0.25° and 0.5° divergence) and the diffracted (7.5 mm height) beam. Variable temperature (VT) X-ray powder diffraction patterns were collected on **1** in the 298-773 K temperature range with steps of 25 K using an Anton Paar HTK 1200N Oven camera. The measurements were carried out at ambient pressure under a mild N_2 flow, at a heating rate of 10 K min^{-1}. Thermogravimetric analysis measurements were performed under N_2 atmosphere (100 mL min^{-1}) at a

heating rate of 10 K min^{-1} on an EXSTAR Thermo Gravimetric Analyzer (TG-DTG) Seiko 6200. NMR spectra were recorded on a BRUKER AVANCE II 300 spectrometer. ^{1}H and $^{13}C\{^{1}H\}$ chemical shifts are reported in parts per million (ppm) downfield of tetramethylsilane (TMS) and were calibrated against the residual resonance of the protiated part of the deuterated solvent. FT-IR spectra (KBr pellets) were recorded on a Perkin-Elmer Spectrum BX Series FTIR spectrometer, in the 4000−400 cm^{-1} range, with a 2 cm^{-1} resolution. The C, H, N, S elemental analyses were made at ICCOM-CNR using a Thermo FlashEA 1112 Series CHNS-O elemental analyzer with an accepted tolerance of ± 2% on carbon (C), hydrogen (H), nitrogen (N) and sulfur (S). ESI-MS spectra were recorded by direct introduction (10 μL/min) on a FinniganLTQ mass spectrometer (Thermo, San Jose, CA). The instrument was equipped with a conventional ESI source. The working conditions were the following: positive polarity: spray voltage 5 kV, capillary voltage 35 V, capillary temperature 548 K and tube lens 110 V. Sheath gas was set at 10 a.u. and auxiliary gas was kept at 3 a.u. For acquisition, Xcalibur 2.0 software (Thermo) was used. Methanol sample solutions were acidified with an aqueous formic acid solution (0.1%) and diluted to 20 ng/μL. GC-MS analyses were performed on a Shimadzu QP2010S apparatus equipped with a Supelco SPB-1 fused silica capillary column (30 m length, 0.25 mm i.d., 0.25 mm film thickness). The amount of zirconium leached in solution after catalysis was determined by Grafite Furnace Atomic Absorption Spectroscopy (GF-AAS) on a GBC 908AA instrument.

Synthesis of [2,2'-bithiazole]-5,5'-dicarboxylic acid (H_2TzTz). A freshly prepared NaOH 1M aqueous solution (20 mL) was added to a suspension of diethyl [2,2'-bithiazole]-5,5'-dicarboxylate (650 mg, 2.081 mmol) in methanol (20 mL), and the resulting mixture was left stirring at ambient temperature overnight. After that time, a clear yellow solution formed and TLC analysis (petroleum ether/ethyl acetate 5:1) showed no more ester starting material. Methanol was removed by rotary evaporation and the residual aqueous phase was acidified with HCl 1M until very low pH values (3-4). During HCl addition, **1** starts to precipitate and the reaction flask was left at low temperature (277 K) for some hours in order to facilitate the precipitation. The yellow solid recovery was achieved through filtration on filter paper. Single crystals

suitable for X-ray diffraction analysis were obtained from a cold (277 K) water/methanol (1:1) concentrated solution. The single-crystal X-ray diffraction data acquisition and treatment as well as the molecular structure are reported in the Supporting Information (Figure S1 and Table S1). Yield 74%. Elem. Anal. Calc. for $H_2TzTz \cdot H_2O$, $C_8H_6N_2O_5S_2$ (MW = 274.27 g/mol): C, 35.03; H, 2.20; N, 10.21%; S, 23.38. Found: C, 35.38; H, 2.34; N, 10.03%; S, 23.41. ESI-MS/MS: *m/z* = 257 $(M+H)^+$, *m/z* = 213 $(M+H-CO_2)^+$, *m/z* = 169 $(M+H-2CO_2)^+$. IR (KBr pellet, cm^{-1}): 3448 (s, br) [ν(O-H)], 3104 (w) [ν(C-H)], 1704 (vs) [ν(C=O)], 1513 (m) [ν(C=C)], 1420 (m), 1369 (m), 1314 (s), 1254 (vs), 1161 (m) [ν(C=N)], 1095 (w), 944 (w), 905 (w), 750 (m) [γ(C-H)], 612 (w) [ν(C-S)], 482 (w). ^1H NMR (300 MHz, D_2O, 298 K, δ, ppm): = 7.84 (2H, C*H*). ^{13}C NMR (75 MHz, CD_3OD, 298 K, δ, ppm)[14]: 166.87 (COOH), 162.57 (C^2), 145.52 (C^4), 139.56 (C^5).

Synthesis of $[Zr_6O_4(OH)_4(TzTz)_6]\cdot 4(DMF)$ (1·DMF). Following the improved preparation of UiO-67 reported by Fahra *et al.*,[15] zirconium chloride [$ZrCl_4$, 0.091 g, 0.39 mmol] and a concentrated (12 M) HCl aqueous solution (0.5 mL) were mixed together and diluted with *N,N*-dimethylformamide (DMF, 5 mL). The resulting suspension was sonicated in an ultrasonic bath at ambient temperature for 15 minutes. After that time, the ligand H_2TzTz (0.100 g, 0.39 mmol) was added to the clear colorless solution; the mixture was further diluted with fresh DMF (10 mL), sonicated for additional 15 minutes and finally transferred to a Teflon-lined stainless steel autoclave (inner Teflon beaker volume ca. 20 mL). The autoclave was sealed and heated at 358 K for 24 h under autogenous pressure. After slow overnight cooling, a microcrystalline yellow powder of **1·DMF** formed at the bottom of the beaker. It was collected, washed with ethanol (4 x 10 mL), petroleum ether (4 x 10 mL) and finally dried under a nitrogen stream at room temperature. Yield: 0.134 g (82.5%). The phase purity was checked every time through PXRD. Elemental analysis calcd (%) for **1·DMF**, $C_{60}H_{44}N_{16}O_{36}S_{12}Zr_6$ (MW = 2497.20 g/mol): C 28.86, H 1.78, N 8.97, S 15.41; found: C 28.51, H 1.66, N 8.78, S 15.37. IR bands (KBr, cm^{-1}): 3411 (s) [ν(O-H)], 3084 (m) [ν(C-H)], 2933 (m) [$\nu(C\text{-}H)_{DMF}$], 1658 (vs) [ν(C=O)], 1595 (vs) [$\nu(C{=}O)_{DMF}$], 1507 (s) [ν(C=C)],

1402 (vs) [ν(C-N)$_{DMF}$], 1254 (m), 1145 (m), 1103 (m), 1022 (w), 933 (m), 889 (w), 770 (m) [γ(C-H)$_{DMF}$], 646 (s) [ν(C-S)], 458 (m).

Powder X-ray Diffraction Structure Determination. Data acquisition was performed at 298 K in transmission scan mode at 40kV and 30 mA, at a STOE STADI P diffractometer (STOE, Darmstadt, Germany) equipped with a Cu-Kα_1 radiation source (λ = 1.5418 Å). Diffraction datasets for a full structure characterization were collected in the 2° – 80° 2θ range, with steps of 0.1° (collection time: 24 sec per step). Structure refinement of the framework was carried out with the Rietveld[16] least squares method as implemented in the FullProf software suite (http://www.ccp14.ac.uk/ccp/web-mirrors/fullprof/index.html) starting from the crystal structure of the isostructural bis(thiophene) MOF [$Zr_6O_4(OH)_4(ThTh)_6$].[17] The atomic coordinates were let vary without constraints and with fixed U_{iso} during the refinement. The chlatrated DMF molecules were refined as rigid body groups. The final refinement plot is shown in Figure S2. The pertinent CIF file is supplied as Electronic Supplementary Information. Crystallographic data for **1·DMF**: $C_{48}H_{16}N_{12}O_{32}S_{12}Zr_6$·4DMF, MW = 2497.20 g mol^{-1}, cubic, $Pn\overline{3}$, a = 25.3505(8) Å, V = 16291.4(9) Å^3, Z = 4, ρ = 1.60832 g cm^{-3}, R_p = 5.93 and R_{wp}= 7.98, for 1941 data and 123 parameters. CCDC-1883540.

Gas Adsorption. All the samples were washed with hot acetone (323 K, 3 x 15 mL) and dried at 353 K under high vacuum (10^{-6} Torr) for 12 h before each measurement. The Brunauer−Emmett−Teller (BET) area and porosity were estimated by volumetric adsorption carried out with an ASAP 2020 Micromeritics instrument, using N_2 as adsorbate at 77 K. A typical measurement used 40 mg of sample. For the BET calculation, the 0.01-0.1 p/p* pressure range for the data fitting was used. Within this range, all the Rouquerol consistency criteria[18] are satisfied. The micropore size distribution was determined through the non-local density functional

theory method (NLDFT - cylinder-like pore shape typical of inorganic oxide materials). The micropore area was evaluated through the *t*-plot method with the Harkins and Jura thickness equation, while the micropore volume was estimated through the application of the Dubinin-Astakhov model to the N_2 isotherm in the $0 \leq p/p^* \leq 0.02$ range.[19] CO_2 adsorption isotherms were recorded at 273 and 298 K at a maximum pressure of 1.2 bar, while the N_2 adsorption isotherm for the determination of the CO_2/N_2 selectivity was recorded at 298 K and up to 1.2 bar. The isosteric heat of adsorption (Q_{st}) was calculated from the CO_2 isotherms measured at 273 and 298 K according to a variant of the Clausius-Clapeyron equation: [20]

$$\ln\left(\frac{p_1}{p_2}\right) = Q_{st} \times \frac{T_2 - T_1}{R \times T_1 \times T_2} \qquad \text{(Equation 1)}$$

where p_n (n = 1 or 2) is the pressure value for isotherm n; T_n (n = 1 or 2) is the temperature value for isotherm n; R is the gas constant (8.314 J K^{-1} mol^{-1}). The CO_2/N_2 selectivity at 298 K based on the Henry method was calculated as the ratio of the initial slopes of the adsorption isotherms. The IAST selectivity for an equimolar CO_2/N_2 mixture at a total pressure of 1 bar was determined as the ratio of the (adsorbed) molar fractions of the two gases[21] as derived from the application of the free software pyIAST (https://github.com/CorySimon/pyIAST)[22] to the experimental N_2 and CO_2 isotherms of **1** collected at 298 K. A Dual-Site Langmuir (CO_2) and a Henry (N_2) model were employed for the isotherm fitting, with root mean square deviation = 0.015 (K_1 = 0.082; K_2 = 0.027; M_1 = 21.24; M_2 = 2.42) and 0.004 (K_H = 0.211), respectively. For a detailed explanation of these parameters, see the pyIAST webpage and documentation.

Computational Methodology. The topologically based crystal constructor (ToBaCCo) code[23] was used to generate twelve MOF structures from the thiazole linker H_2TzTz. The ToBaCCo 2.0 code from Argueta *et al.*[24] includes a molecular building block-based charge assignment scheme, which assigns partial charges to the MOF structure based on the partial charges of the node and linker building blocks. MOF structures were generated using all combinations of metal nodes from Argueta's study that were

chemically compatible with the dianionic nature of $TzTz^{2-}$. Partial charges were assigned to an isolated thiazole linker using the ChELPG charge assignment scheme[25] in *Gaussian 16*[26] following the same methodology of Argueta *et al.* for consistency.[24] The linker was considered in its protonated form for charge calculations. The B3LYP functional[27] and 6-31+G* basis set[28] were employed for non-metal atoms and the LANL2DZ basis set and pseudopotential[29] were used for metals, in order to be consistent with the computational methodology chosen by Argueta and coworkers,[24] by other DFT calculations performed on thiophene-based MOFs[30] and by other similar calculations.[31] After calculating partial charges for the linker molecule, we used the ToBaCCo code to construct the twelve MOF structures *in silico* and map the partial charges from the building blocks onto the generated framework structures. Then, the Forcite module in Materials Studio[32] was exploited to geometrically optimize the crystals using a two-stage approach. Initially, the structure was relaxed keeping fixed lattice parameters, and in a second stage the unit cell was also allowed to relax. These relaxations used the Universal Force Field (UFF)[33] for molecular mechanics and the "smart" optimizer, which uses a cascade of steepest descent, conjugate gradient, and quasi-Newton methods. Isotherms were simulated with grand canonical Monte Carlo (GCMC) simulations in RASPA.[34] CO_2 calculations were run using 5,000 cycles for equilibration and 5,000 for production data. Points along the N_2 isotherm were calculated using 20,000 cycles for equilibration and 20,000 cycles for production. These simulation lengths are consistent with prior literature[35] to achieve small error bars. UFF[33] was used to assign Lennard-Jones parameters to the framework atoms and Lorentz-Berthelot mixing rules for cross-terms with the adsorbates. The N_2 and CO_2 guest molecules were simulated using the relevant TraPPE force field parameters.[36] Guest-guest charges were included for both adsorbates, and host-guest electrostatics were included for CO_2. See Table S2 for the parameters list.

Catalytic CO_2 Cycloaddition to Epoxides with 1. Before the catalytic trials, **1·DMF** was washed with hot acetone (323 K, 3 x 15 mL), dried at 353 K under high vacuum (10^{-6} Torr) for 12 h and then stored under N_2 atmosphere. The activated MOF catalyst **1** (0.05 mmol Zr) and the epoxide substrate (20 mmol) were placed in a Teflon sample holder inside a stainless steel reactor under an inert atmosphere.

The reactor was then pressurized with CO_2 (p = 1 atm) and kept at the chosen temperature (363 or 393 K) for 24 h under stirring. CO_2 was continuously fed to maintain the reactor pressure constant. At the end of the reaction, the reactor was cooled in an ice/water bath and bis(2-chloroethyl) ether (20 mmol) was added to the mixture as internal standard. The as-obtained MOF-suspension was filtered over a Celite pad and liquid products analyzed by GC-MS. For the recycling tests, after the first catalytic run the supernatant was carefully removed under an inert atmosphere. The solid catalyst was washed with dry and degassed acetone (3 × 5 mL) and it was then dried under vacuum for 1 h to remove volatiles before re-using it in further catalytic tests.

Results and Discussion

Synthesis of H_2TzTz and computer-aided MOF screening for CO_2 adsorption. The dicarboxylic acid H_2TzTz was prepared through basic hydrolysis of the corresponding diethyl ester. The latter was obtained from a Pd/Cu-catalyzed [2,2′]-homocoupling of the commercially available (Sigma Aldrich) ethyl thiazole-5-carboxylate, following a literature procedure.[13] Acidification of the aqueous solution containing the sodium dicarboxylate salt led to precipitation of H_2TzTz as a hydrate (with a variable water content) at pH ≈ 4 in fairly good yield (for the crystal structure see the Supporting Information).

After the development of a consolidated and reproducible methodology for the ligand synthesis, a computational approach was applied to select a MOF target for synthesis using H_2TzTz as ditopic linker, thus saving synthetic effort. Broadly speaking, computational-experimental joint investigations represent a powerful approach to materials design, leveraging the rapid prototyping capabilities of simulation in conjunction with synthetic experience and characterization from experiment. Geometric algorithms can construct thousands of MOF structures *in silico*, which are then studied with high-throughput molecular simulations to identify the best candidates for experimental verification.[23, 35, 37] These methods have also been used at a smaller scale, generating dozens of structures instead of thousands, to assist in understanding experimental results, *e.g.* generating simulated PXRDs to resolve complex crystal structures, or to limit the number of synthetic efforts required to prepare MOFs for target applications.[38]

We wanted to find the combination of transition metal nodes and topology yielding the best MOF material for CO_2 uptake at ambient temperature and pressure using H_2TzTz as a linker. To answer this question, we used the topologically-based crystal constructor (ToBaCCo) algorithm[23] to construct *in silico* a dozen MOF options, with assorted edge-transitive crystal topologies (**acs, bcs, bcu, crs, fcu, lvt, nbo, pcu, reo, rhr, ssa, ssb**)[39] and metal ions (Zr^{IV}, Cr^{III}, Zn^{II}, Cu^{II}). We selected these MOF blueprints from the previously published ToBaCCo library, using the metal corners and topologies compatible with the dicarboxylate coordination of the H_2TzTz linker. Illustrative pictures of the three-dimensional connectivity of these MOFs are reported in the Supporting Information (Figure S3), along with the corresponding optimized CIF files. Subsequently, all the geometrically optimized structures were further studied through grand canonical Monte Carlo (GCMC) simulations of CO_2 adsorption using the RASPA code.[34] The output of GCMC calculations revealed that, among the options taken into account, the Zirconium MOF of **fcu** cubic topology isostructural with those coming from the UiO family[40] and containing the [Zr_6] octahedral metal cluster as a node is the best-performing material for carbon dioxide adsorption (the calculated CO_2 adsorption isotherms up to 1.2 bar pressure are reported in Figure S4 for all 12 structures). On the basis of the simulation results, the experimental efforts were focused on the preparation of the zirconium MOF, which also has the advantage of higher thermal and chemical stability compared with some of the other MOFs. Group 4 transition elements interact strongly with oxygen and are therefore obvious choices for stable inorganic cornerstones in combination with oxygen containing linkers.[41]

Synthesis and structure of $[Zr_6O_4(OH)_4(TzTz)_6]\cdot 4(DMF)$ (1·DMF). $[Zr_6O_4(OH)_4(TzTz)_6]$ was prepared under solvothermal conditions starting from anhydrous $ZrCl_4$, following a well-established experimental protocol for the synthesis of highly crystalline samples of other zirconium MOFs of the UiO family in *N,N*-dimethylformamide (DMF) as solvent of choice.[15] The use of concentrated HCl (12 M, 37% aqueous solution) as crystal modulator led to a far better product (in terms of crystallinity degree) than those obtained using other modulators like L-proline[42] or weaker organic acids like acetic acid,

formic acid or benzoic acid,[43] where only amorphous phases were obtained instead. Similarly, the simple metacrylate^{-} → $TzTz^{2-}$ ligand exchange using the commercially available (Sigma Aldrich) $[Zr_6O_4(OH)_4(metacrylate)_{12}]$ Secondary Building Unit (SBU) as starting reagent under the same solvothermal conditions in a 1:1 stoichiometric ratio with H_2TzTz led to an amorphous product. Unfortunately, no crystals suitable for single-crystal X-ray structural solution were grown from the reaction mixture, despite the numerous attempts made. Dilution of the reaction mixture simply led to a lower product yield, but without improvement in terms of crystal size. Therefore, the structure was solved from powder X-ray diffraction (PXRD) data (Figure 1). **1·DMF** crystallizes in the cubic space group $Pn\overline{3}$ and it is isoreticular[44] with the members of the UiO family[40] and also with the bithiophene analogue of general formula $[Zr_6O_4(OH)_4(ThTh)_6]\cdot n(DMF)$ ($ThTh^{2-}$ = [2,2'-bithiophene]-5,5'-dicarboxylate).[17] The Zr-oxo cluster SBU is surrounded by twelve carboxylate groups coming from six different ditopic $TzTz^{2-}$ bridging linkers, resulting in a 3D open framework very similar to that of UiO-67 ($[Zr_6O_4(OH)_4(PhPh)_6]$, where $PhPh^{2-}$ = biphenyl-4,4'-dicarboxylate). Each zirconium atom is eight-coordinated forming a square-antiprismatic coordination consisting of eight oxygen atoms. One square face is formed by oxygen atoms supplied by carboxylates while the second square face is formed by oxygen atoms coming from the μ_3-O and μ_3-OH groups. The biphenyl-4,4′-dicarboxylate ligand in UiO-67 has a linear shape, whereas the non-linear nature of $TzTz^{2-}$ [angle between the two $-COO^{-}$ groups ≈ 175°] is at the origin of the slightly different space group of the resulting MOF ($Fm\overline{3}m$ and $Pn\overline{3}$ for UiO-67 and **1·DMF**, respectively). The same reduction of symmetry in $[Zr_6]$ MOFs of cubic topology is also observed in other cases where non-linear linkers like fumaric,[45] hexa-2,4-dienoic[46] and napthtalene-2,6-dicarboxylic[47] acid are used. The $TzTz^{2-}$ ligand is in the same conformation as that found in its free form (*trans* reciprocal disposition of the N and S atoms on the two heterocyclic rings; see also Figure S1 in the Supporting Information). **1·DMF** contains two types of cages: an octahedral cage that is face-sharing with eight tetrahedral cages, and edge-sharing with eight additional octahedral pores. An empty cell volume of 62 % was estimated with the software PLATON[48] after removal of the clathrated solvent. This translates into a theoretical

pore volume of 0.69 cm^3/g. The mean Zr-O(carboxylate) distance in **1·DMF** (2.18 Å) is in line with those found in other UiO-67-type MOFs from the literature (mean Cambridge Structural Database (CSD) value = 2.23 Å).[49] Four crystallographically distinct chlatrated DMF solvent molecules were located within the octahedral cavities. Figure S2 shows the result of the Rietveld refinement on the PXRD pattern of **1·DMF**. The topological analysis of the crystal lattice performed through the TOPOS 4.0 software[50] confirms the calculated **fcu** network topology (taking the $[Zr_6]$ clusters as nodes and $TzTz^{2-}$ as connector).

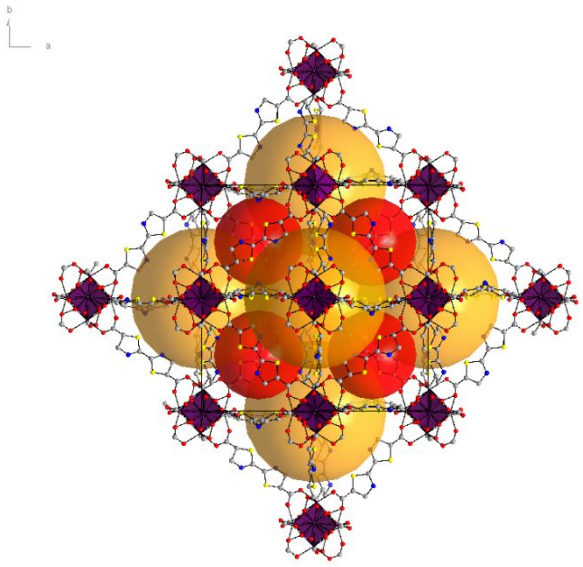

Figure 1. Crystal structure of **1·DMF**: portion of the packing, viewed in perspective along the *c* crystallographic direction. Atom color code: grey, C; red, O; blue, N; yellow, S; purple, Zr. The solvent molecules and hydrogen atoms have been omitted for clarity. The golden and red spheres indicate the octahedral and tetrahedral crystal cavities, respectively.

Thermal Behavior. A combined thermogravimetric / mass spectrometry (TG-MS) and variable-temperature powder X-ray diffraction (VT-PXRD) analysis was carried out to assess the thermal stability and the crystalline scaffold robustness of **1·DMF**. The MOF is stable up to 673 K under N_2 atmosphere. The decomposition temperature is the same under air (Figure S5), proving that **1** is stable under oxidative environment. The TG profile (Figure 2a) shows a weight loss of ~12.0% between 373 and 523 K, corresponding to four DMF chlatrated molecules (theoretical loss: 11.7 %). At the same time, some of DMF typical fragmentation peaks falling at *m/z* = 72-74 a.m.u. grow on the MS profile of the volatiles (Figure S6 in the Supporting Information). Nevertheless, no stable solvent-free phase could be found on

the TG profile, since after solvent loss a progressive decomposition takes place until 773 K, with concomitant growth of other fragmentation peaks at *m/z* = 84-86 a.m.u. (thiazole) on the MS profile of the volatiles (Figure S6). The solid residue at high temperature was found to be the mixed oxide-sulfide cubic phase $Zr(O_{1.6}S_{0.4})$, judging from the peaks growing from the amorphous at T = 773 K (Figure 2b),[51] even though the weight residue of *ca.* 35 % found on the TG profile (Figure 2a) better fits with a hypothetical $[2(ZrO_2) + 4(ZrS_2)]$ composition (theoretical residue: 34.7 %). The decomposition temperature of **1** is lower than that of UiO-67 (813 K)[40] but slightly higher than that of its thiophene analogue $[Zr_6O_4(OH)_4(ThTh)_6]$ (663 K),[17] in line with the basicity trend in the corresponding monocarboxylate species.[52] Despite its relatively high thermal stability, **1** suffers from loss of crystallinity at temperatures higher than 423 K, as witnessed by the VT-PXRD profiles recorded under N_2 flow (Figure 2b). The complete removal of the solvent causes a framework collapse and loss of microporosity, leaving an amorphous phase. This is in agreement with the N_2 adsorption experiments that provide a BET area of the real sample lower than the theoretical upper limit evaluated for a perfectly crystalline empty framework (see the N_2 adsorption Section). Despite the various attempts made, we were unable to achieve a thorough DMF removal from the MOF pores. The process is probably hampered by the existence of strong hydrogen bonding interactions between the N heteroatoms on the thiazole rings and DMF, that is not present in the case of the thiophene analogue $[Zr_6O_4(OH)_4(ThTh)_6]$.[17]

(a) (b)

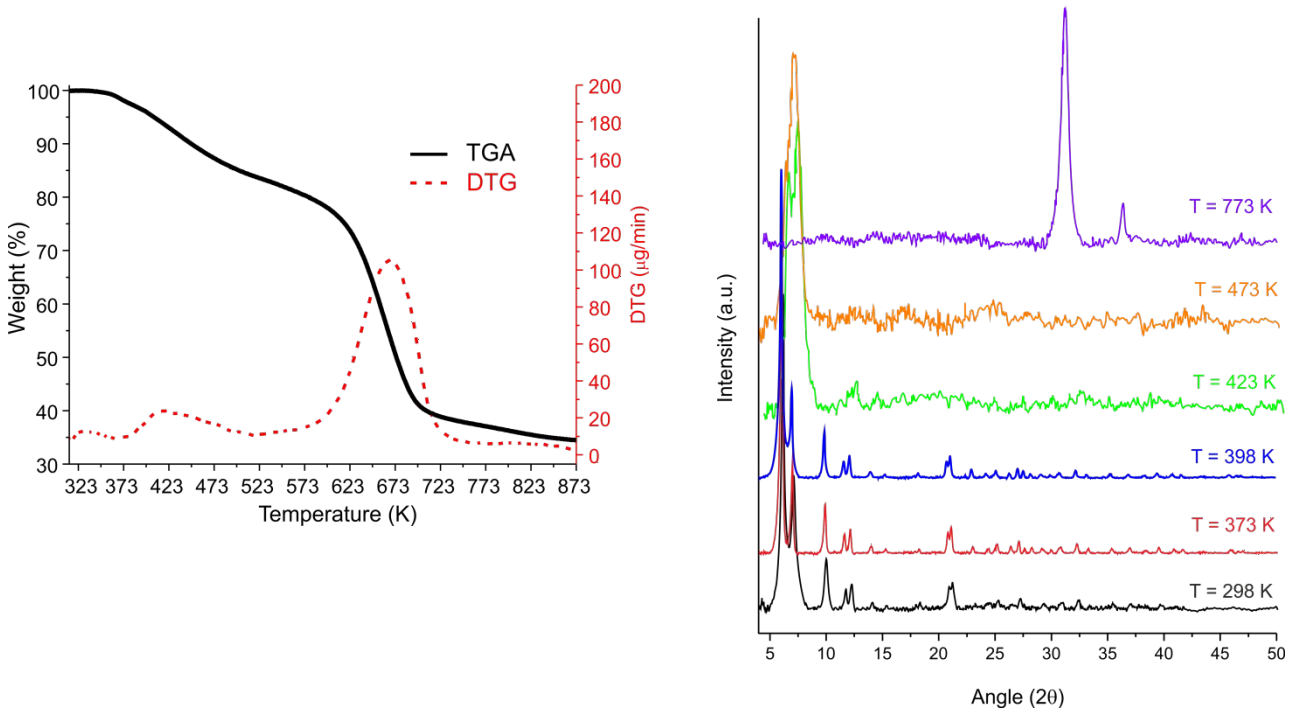

Figure 2. Thermal behavior of **1**·**DMF**: (a) TGA-DTG traces (solid and dotted line, respectively). For the related MS fragmentation peaks, see Figure S5 in the Supporting Information. (b) Selected PXRD patterns measured as a function of temperature heating in N_2.

N_2 Adsorption. The porous nature of the synthesized MOF was investigated through N_2 adsorption measurements at 77 K after repeated hot acetone washings (323 K) and mild thermal activation at 353 K under high vacuum (10^{-6} Torr) for 12 h. As shown in Figure 3a, **1** shows a type I isotherm, typical of a microporous material, with a BET area of 840 m^2/g. This value is much lower than those found for UiO-67 (2505 m^2/g)[40] or for $[Zr_6O_4(OH)_4(ThTh)_6]$ (2207 m^2/g),[17] because of the impossibility to remove the DMF solvent thoroughly from the inner cavities without causing a structural collapse (see also the Thermal Behavior Section above). In line with this finding, the pore volume per cell of 0.69 cm^3/g calculated from the crystal structure (*vide supra*) is much higher than the limiting micropore volume estimated through the application of the Dubinin-Astakhov model to the N_2 adsorption isotherm of the real sample (0.32 cm^3/g). Therefore, the latter is only partially activated (*ca.* 46 % of the theoretical micropore volume is indeed accessible). A more precise measurement of the

amount of DMF removed after activation comes from the TGA-MS analysis carried out on the activated sample **1** (Figure S7). A weight loss of *ca.* 6.5% is found on the TG profile of **1** in the 450 – 550 K temperature range, with *m/z* peaks equal to 72-74 a.m.u. typical of DMF appearing on the mass spectrum. This loss corresponds to approximately 55% of the initial weight loss measured on **1·DMF** (12.0 %), in line with the information coming from the N_2 adsorption isotherm at T = 77 K. The total pore volume evaluated at p/p* = 0.95 equals 0.38 cm^3/g. The Dubinin-Astakhov analysis also revealed that the micropore volume represents the main contribution to the total pore volume (84%). In **1**, there are two different micropore sizes (retrieved from the DFT analysis – cylindrical pore shape of inorganic oxide materials) of 1.5 and 1.9 nm.

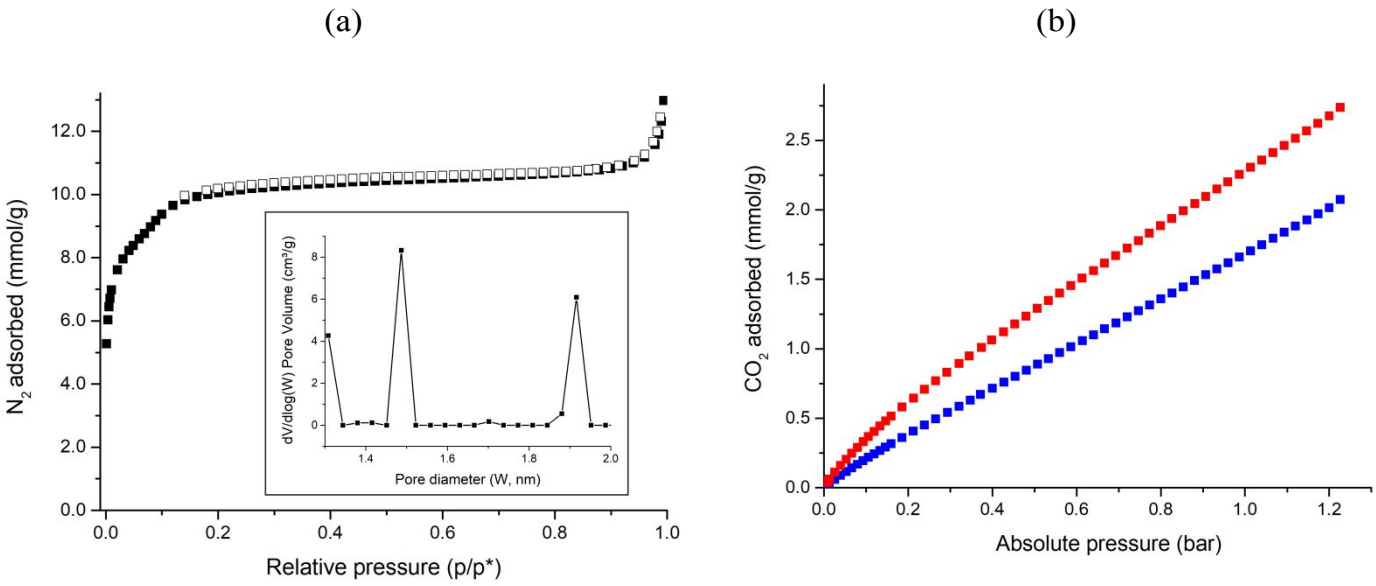

Figure 3. (a) N_2 adsorption isotherm (black squares) measured at 77 K on **1**. The desorption branch is drawn with empty symbols. Inset: NLDFT micropore size distribution as derived from the experimental isotherm. (b) CO_2 adsorption isotherms measured at 298 K (blue squares) and 273 K (red squares) on **1**.

CO_2 Adsorption. 1 was tested as a CO_2 adsorbent at T = 273 and 298 K and at p_{CO2} up to 1.2 bar. The corresponding isotherms are reported in Figure 3b. The amount of gas adsorbed at 298 K and 1 bar is 7.5 wt.% CO_2, corresponding to 1.7 mmol/g. As expected, the presence of a basic N atom on the skeleton of $TzTz^{2-}$ does favor CO_2 adsorption through non-covalent interactions

between the exposed N atoms and CO_2. The adsorption capacity and the surface area are comparable to those of UiO-67-IL, a derivative where the biphenyl linker of the pristine MOF has been functionalized with an imidazolium salt, thus increasing the number of acidic interaction sites.[53] This reveals a strong affinity of **1** for CO_2.

Compound	CO_2 uptake [mmol/g]		BET area [m^2/g]	Q_{st} [kJ/mol]	Ref.
	273 K	298 K			
1	2.3	1.7	840	18.7	This work
UiO-67	2.2	0.9	2505	15.9	[49f]
$[Zr_6O_4(OH)_4(ThTh)_6]$	4.0	3.1	2207	18.4	17
BUT-10		2.1	1848	21.8	[49f]
BUT-11		2.2	1310	25.9	[49f]
BUT-11-AcOH	4.8	2.9	1452	26.5	[54]
BUT-11-HCl	4.1	2.4	1456		[54]
UiO-67-$(NH_2)_2$	2.7	1.2	1360	25.5	[55]
UiO-67-IL	2.1	0.9	846	27.0	[53]

Table 1. Comparison of CO_2 uptake (at 1 bar and 273 and/or 298 K) and isosteric heat of adsorption (Q_{st}) among representative UiO-67-like zirconium MOFs of the *state-of-the-art*. When directly unavailable from the literature, the values were calculated from the presented results (if possible).

To quantify the strength of the CO_2-MOF interactions in **1**, the isosteric heat of adsorption (Q_{st}) of CO_2 was evaluated with a variant of the Clausius-Clapeyron equation, through the comparison of the isotherms recorded at 273 and 298 K. The isosteric heat of adsorption reflects the interaction strength between CO_2 and the inner pore walls of **1**. The value of 18.7 kJ/mol calculated at zero coverage is higher than that estimated for UiO-67 (15.9 kJ/mol)[49f] and it is almost identical to that of the thiophene analogue $[Zr_6O_4(OH)_4(ThTh)_6]$ (18.4 kJ/mol).[17] On the other hand, the heat of adsorption measured for **1** is lower than those measured on sulfone-[54] or amino[55]-functionalized UiO-67

MOFs, because of the much higher polarity (-SO_2) or basicity (-NH_2) of these functional groups compared with thiazole. We estimated the CO_2/N_2 selectivity using the ratio of the initial slopes in the Henry region of the related adsorption isotherms measured at 298 K (Figure S8): **1** shows a CO_2/N_2 selectivity of 10, comparable to that of UiO-67 (9.4).[49f] The IAST CO_2/N_2 selectivity value for an equimolar mixture measured at p = 1 bar is 8.4; this value is also comparable to that found for UiO-67.

Adsorption isotherms and primary CO_2 adsorption sites from simulation. GCMC simulations were run on **1** with the aim of casting light on the adsorption mechanism in this MOF. To better understand the textural properties, **1** was also characterized using Zeo++[56] with an N_2 probe of 3.72 Å diameter. The experimental saturation loading of N_2 in **1** is ~52% of the simulated value from GCMC, which is reasonably close to the percentage found through the Dubinin-Astakhov evaluation of the accessible micropore volume (46%). In line with this finding, the real Langmuir surface area (around 1000 m^2/g) is half of the theoretical one (2083 m^2/g) evaluated from a perfectly evacuated crystalline sample. At the same time, given the inverse proportionality between surface area and pore diameter (W = 4V/S), the micropore size found from the experimental isotherm through NLDFT modeling (1.5 and 1.9 nm) is roughly twice as much as that evaluated from purely geometrical considerations with the method of Gelb and Gubbins[57] starting from the crystal structure (0.8 and 1.0 nm, inset of Figure 4a). This discrepancy between experiment and simulation is normally ascribed to pore collapse or incomplete activation of the real sample,[58] with concomitant reduction of its accessible surface area if compared with the theoretical upper limit that is calculated on a perfectly empty and regular crystalline scaffold. The geometric properties and linker length are collected in Table 2, while the simulated N_2 isotherm is reported in Figure 4a.

Table 2. Calculated textural properties of **1**.

Linker	Carboxylates distance [Å]	Unit cell volume [Å^3]	Volumetric BET area [m^2/cm^3]	Gravimetric BET area [m^2/g]	Density [g/cm^3]
TzTz	9.0	15474	1972	2083	0.95

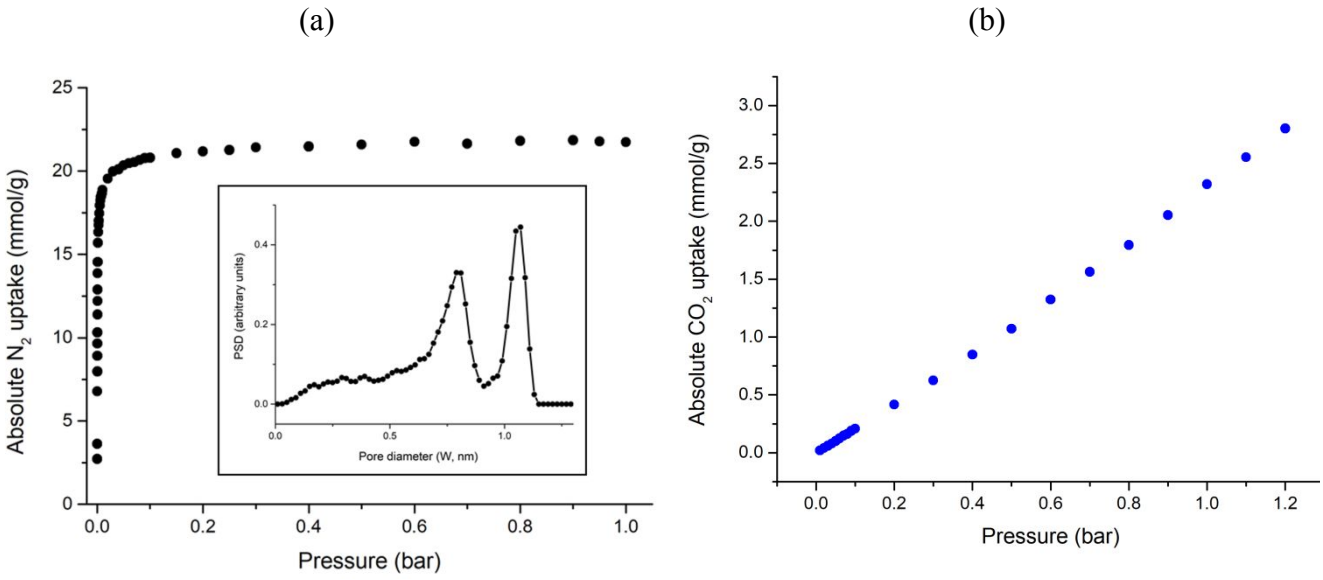

Figure 4. GCMC simulated adsorption isotherms of **1** for N_2 at 77 K (a) and CO_2 at 298 K (b). Inset of Figure 4a: simulated pore size distribution evaluated through geometrical considerations from the crystal structure.

The simulated CO_2 isotherm for **1** is depicted in Figure 4b. The simulations give a predicted value of 2.80 mmol/g of CO_2 adsorbed at p = 1.2 bar and T = 298 K. Again, the calculated uptake is higher than the experimental one (2.80 *vs.* 2.07 mmol/g, respectively), because of incomplete framework evacuation.

Figure 5 shows simulation snapshots of CO_2 molecules sitting within the channels of **1**, visualized using VMD.[59] The primary adsorption sites determined computationally are the heteroatoms within the linkers in the corners of the channels. This is also in agreement with the DFT-calculated partial atomic charges for the H_2TzTz linker (Figure S9). From its electrostatic potential map, it can be inferred that sulfur has a nearly zero partial charge, but the incorporation of an N atom in the skeleton of H_2TzTz creates a nucleophilic anchoring site for the capture of the electrophilic CO_2 guest. Radial Distribution Function (RDF) plots (Figure S10) between selected framework atoms and the carbon atom in the adsorbed CO_2 molecule show probability maxima at r ~ 4.7 Å for the MOF nitrogen atom, 4.2 Å for the sulfur atom, and 4.0 Å for the center of the heterocyclic ring. The strong peak for the first coordination shell provides additional evidence for preferential CO_2 adsorption near the five-membered ring on the linker. From simulation, the calculated heat of adsorption for CO_2 in **1** is 20-22 kJ/mol (Figure S11), which is in reasonable agreement with the experimentally determined value of 19 kJ/mol.

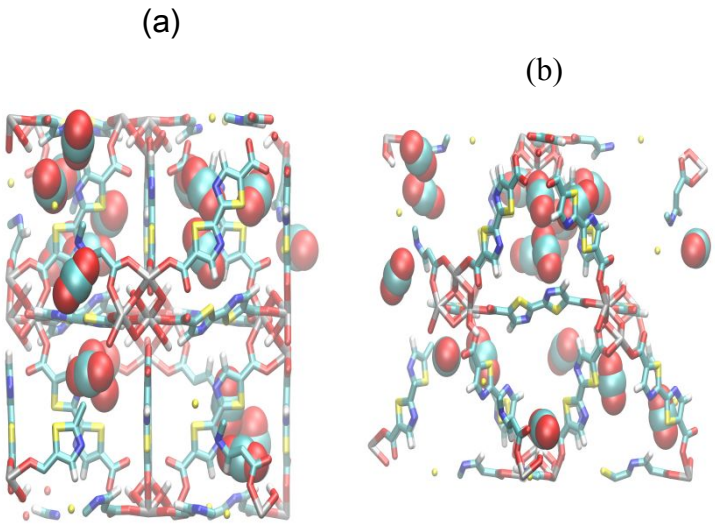

Figure 5. GCMC snapshots of the distribution of CO_2 within the structural models of **1**. The MOFs are viewed along the [001] direction (down the *c* crystallographic axis) in (a) and [101] direction in (b). Atom color code: oxygen (red), carbon (aquamarine), hydrogen (white), sulfur (yellow), nitrogen (blue), zirconium (gray).

Catalytic CO_2 Transformation with 1. The MOF was additionally employed as heterogeneous catalyst for promoting the CO_2 inclusion into cyclic carbonates under mild and green conditions, *i.e.* in the absence of solvent and any co-catalysts.[60] In Zr-MOF-catalyzed CO_2 cycloaddition to epoxides, literature works classically introduce in the reaction mixture a catalytic amount of either an exogenous nucleophile [*e.g.* the counterion of a quaternary ammonium salt (*i.e.* tetrabutylammonium bromide - TBAB) or a relatively strong base (*i.e.* dimetylamminopyridine - DMAP)][61] or an endogenous one (*e.g.* an imidazolium salt embedded within the MOF linker)[62] to run the process efficiently. To the best of our knowledge, **1** is the first example reported to date of a zirconium-MOF catalyst for this reaction that promotes the process *without any added co-catalyst*. In a preliminary screening, epichlorohydrin and epibromohydrin (Scheme 2) were scrutinized as substrates for the process and the catalytic outcomes are summarized in Table 3.

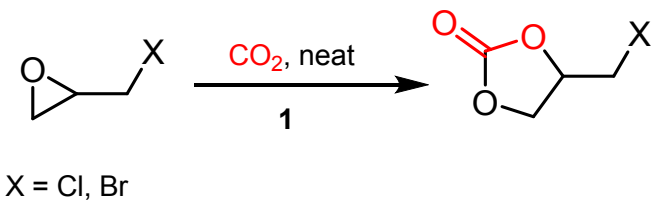

Scheme 2. Catalytic transformation of halogenated epoxides into the corresponding cyclic carbonates examined in this study.

Entry	Catalyst	Exogenous Nucleophile	P [bar]	T [K]	t [h]	Yield [%]	TOF[a]	Ref.
1	**1**	-	1	393	24	61	10.2	this work
2	**1**	-	1	363	24	11	1.8	this work
3[b]	**1**	-	1	393	24	74	12.3	this work
4	(I^-)Meim-UiO-66	-	1	393	12	83.5	9.3	62a
5	UiO-67-IL	-	1	363	3	75	34.2	62b
6	UiO-67	-	1	363	14	8	0.4	62b
7	MOF-53	DMAP	16	373	2	80	398	61d
8	MOF-53	-	16	373	2	0.5	3	61d

Reaction conditions: mmol Zr = 0.05; mmol substrate = 20; [a]calculated as (mmol carbonate)·(mmol Zr)$^{-1}$·h^{-1}; [b]epibromohydrin as substrate.

Table 3. Summary of the catalytic results described in this work and comparison with the literature data for the same catalytic process carried out on zirconium-based MOFs with epichlorohydrin under similar reaction conditions.

The selected temperature and pressure conditions applied in the catalytic trials were identical to those used for a pyrazole-based zinc MOF recently discussed and exploited by some of us in the same process:[63] T = 393 K and p_{CO2} = 1 bar. Under these conditions, the reaction proceeds smoothly with 61 % conversion after 24 h. A reduction of the reaction temperature from 393 to 363 K is found to decrease remarkably the catalyst TOF (expressed as mmol of carbonate produced per mmol of Zr per h) from 10.2 to 1.8 (Table 3, entry 2). Furthermore, under optimized conditions we have observed a slight increase in the substrate conversion for epibromohydrin compared to its chlorinated counterpart (Table 3, entry 1 vs. 3). TOF values obtained for **1** rank in the same order of magnitude as those measured for zirconium MOFs containing endogenous halide ions as co-catalysts for the process like (I^-)Meim-UiO-66[62a] or UiO-67-IL[62b] (Table 3, entries 4 and 5). It is important to note that the presence of a nucleophile is crucial for a successful reaction. A representative example is given for MOF-53, where the authors demonstrate the role played by the co-catalyst (DMAP, see Table 3, entries 8 and 9).[61d] In spite of the relatively harsh reaction conditions (16 bar CO_2 pressure), in the absence of DMAP a drastic reduction of the process efficiency is observed (Table 3, entries 8 *vs.* 9). In the case of **1**, a rational explanation of its catalytic behavior may suppose an active participation of the bis(thiazole) structural motif in the process. Indeed, the basic N-sites of the thiazole rings protruding into the MOF channels interact with CO_2 (in line with the GCMC simulation results) and activate it. At the same time, the Lewis acidic metal nodes foster the epoxide ring-opening according to a commonly accepted mechanistic scheme.[64] Scheme 3 tentatively summarizes the mechanistic path for the CO_2 cycloaddition to with **1** in the absence of any co-catalyst. The reaction is supposed to proceed through the initial intramolecular epoxide ring-opening fostered by the simultaneous push-pull action of the MOF framework that formally behaves as a frustrated Lewis pair. The subsequent carbonate ring-closure takes place through an intramolecular nucleophilic attack, on the basis of a classical addition-elimination sequence. This mechanism is formally similar to that recently proposed by some of us for a pyrazole-based zinc MOF.[63]

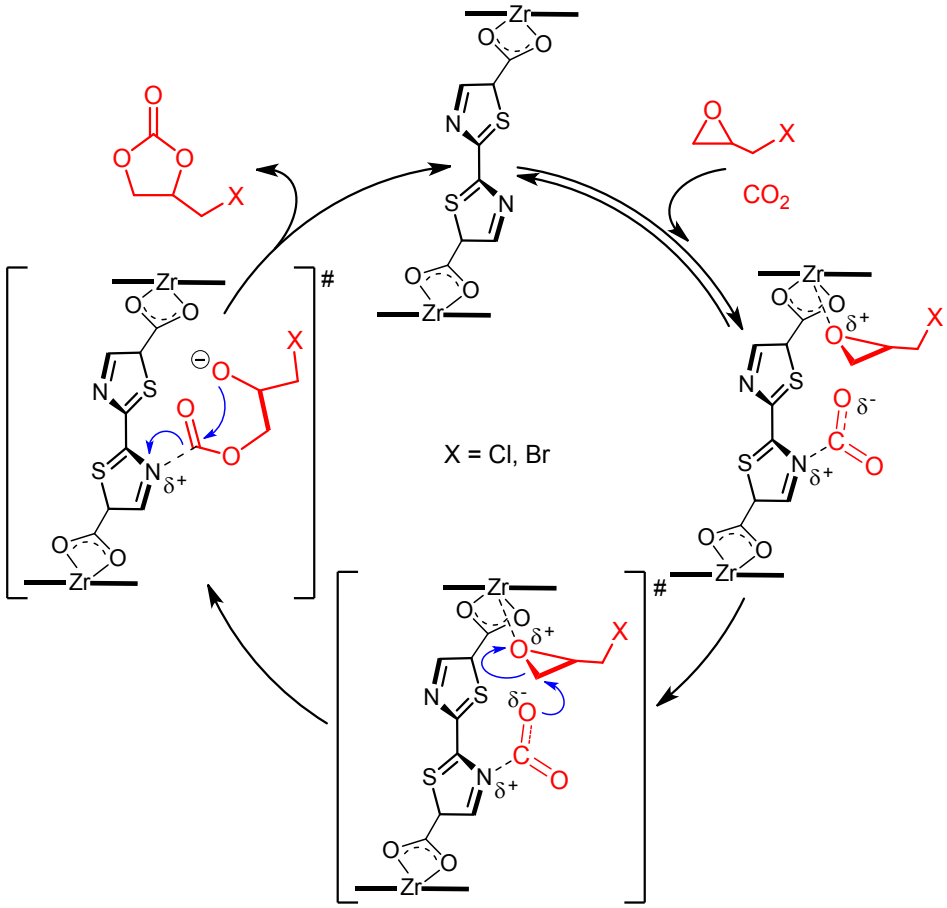

Scheme 3. Proposed mechanistic scheme for the reaction between CO_2 and epihalohydrin catalyzed by **1**.

Catalyst recovery and recycling has also been investigated. **1** maintains its catalytic activity virtually unchanged within three successive runs. Indeed, normalized conversions measured in the three runs are 100%, 99% and 99%, respectively. Recycling tests are straightforwardly accomplished in a dry box under inert atmosphere by recovering the catalyst from the liquid supernatant at the end of each run by centrifugation. The solid is then washed with dry and degassed acetone, filtered and dried under vacuum to constant weight before being treated with an additional amount of epoxide and CO_2. For the sake of completeness, leaching of metal into the reaction supernatant was quantified *via* GF-AAS analysis at the end of each catalytic cycle. The amount of leached zirconium was found to be negligible in all cases with a maximum content of ~0.006% of leached zirconium ions detected in the most contaminated sample. Overall, this confirms the truly heterogeneous nature of the process together with a substantial catalyst

stability throughout several catalytic runs. Finally, the catalyst maintains its crystalline nature after the recycling runs, as confirmed *via* PXRD patterns recorded on the exhaust catalytic material (Figure S12).

Conclusions

The successful combination of computational screening and targeted experimental efforts starting from the organic linker [2,2'-bithiazole]-5,5'-dicarboxylic acid led to the synthesis of a novel MOF material with excellent performance in capturing CO_2 and converting it into cyclic carbonates under mild and green conditions. The microporous zirconium MOF **1** with the same cubic topology as that of UiO-67 was found to be slightly better than its bis(thiophene) analogue $[Zr_6O_4(OH)_4(ThTh)_6]$ ($ThTh^{2-}$ = [2,2'-bithiophene]-5,5'-dicarboxylate) in terms of CO_2 loading capacity, owing to the presence of an extra-N atom in the linker skeleton that enhances the affinity for the acidic carbon dioxide. The GCMC snapshots of the CO_2-loaded **1** revealed that the primary adsorption sites are the heteroatoms within the linkers, confirming the beneficial effect of the increased C-E (E = N, S) bond polarization. The CO_2 trapped into the pores of **1** was subsequently transformed into the cyclic epichlorohydrin and epibromohydrin carbonates through direct and solvent-free reaction with the parent epoxides at ambient pressure and without the assistance of any nucleophilic co-catalyst, with conversions comparable to those found for similar MOFs with endogenous nucleophiles (like imidazolium salts). These results pave the way to the *in silico* design of suitable thiazole-containing MOFs for specific applications in gas separation and green chemistry. This approach is very useful to focus the synthetic efforts on a selected material starting from the *a priori* knowledge of its physico-chemical properties. Other MOF structures chosen from the group of 12 computationally optimized materials may also be interesting targets for synthesis with the aim of achieving a complete pore evacuation (which was not possible in the case of **1**) and higher BET areas to increase the CO_2 uptake capacity. Further studies are ongoing in this direction in our research groups at present.

Conflicts of Interest. R.Q.S. has a financial interest in NuMat Technologies, a startup company that is seeking to commercialize MOFs.

Associated Content

Supporting Information. CIF files of the twelve optimized structures found with the ToBaCCo MOF generator algorithm, of H_2TzTz and **1**. Details on the X-ray diffraction data collection and structure solution and refinement for H_2TzTz. Description of the crystal structure of H_2TzTz. Figures S1-S12, Tables S1 and S2.

Author Information

Corresponding Authors

* Dr. Andrea Rossin. E-mail: a.rossin@iccom.cnr.it

ORCID

Andrea Rossin: 0000-0002-1283-2803

Benjamin Bucior: 0000-0002-8545-3898

Randall Snurr: 0000-0003-2925-9246

Giuliano Giambastiani: 0000-0002-0315-3286

Giulia Tuci: 0000-0002-3411-989X

Stefan Kaskel: 0000-0003-4572-0303

Acknowledgments

G.T. and G.G. thank the Italian MIUR through the PRIN 2015 Project SMARTNESS (2015K7FZLH) for financial support. G.G. thanks the TRAINER project (Catalysts for Transition to Renewable Energy Future) Ref. ANR-17-MPGA-0017 for support. B.B. acknowledges a National Science Foundation Graduate Research Fellowship under Grant No. DGE-1324585. R.Q.S. acknowledges the U.S.

Department of Energy under Award DE-FG02-08ER15967. This research was supported in part through the computational resources and staff contributions provided for the Quest high-performance computing facility at Northwestern University, which is jointly supported by the Office of the Provost, the Office for Research, and Northwestern University Information Technology.

References

1. (a) S. Tiba and A. Omri, *Renewable Sustainable Energy Rev.* 2017, **69**, 1129–1146. (b) P. C. Stern, B. K. Sovacool and T. Dietz, *Nat. Clim. Change* 2016, 547-555. (c) M. Z. Jacobson, *Energy Environ. Sci.* 2009, **2**, 148–173.
2. S. Chu, *Science* 2009, **325**, 1599.
3. Z. Zhang, Z.-Z. Yao, S. Xiang and B. Chen, *Energy Environ. Sci.* 2014, **7**, 2868-2899.
4. (a) L. R. MacGillivray and C. M. Lukehart, *Metal-Organic Framework Materials*, John Wiley & Sons: New York, 2014. (b) B. Seyyedi, *Metal-Organic Frameworks: a New Class of Crystalline Porous Materials*, Lambert Academic Publishing: Saarbrücken, 2014.
5. G. Tuci, A. Rossin, X. Xu, M. Ranocchiari, J. A. van Bokhoven, L. Luconi, I. Manet, M. Melucci and G. Giambastiani, *Chem. Mater.* 2013, **25**, 2297−2308.
6. (a) J. Chen, K. Shen and Y. Li, *ChemSusChem* 2017, **10**, 3165-3187. (b) H. He, J. A. Perman, G. Zhu and S. Ma, *Small* 2016, **12**, 6309–6324.
7. (a) N. Kielland, C. J. Whiteoak and A. W. Kleij, *Adv. Synth. Cat.* 2013, **355**, 2115-2138. (b) M. North, R. Pasquale and C. Young, *Green Chem.* 2010, **12**, 1514-1539. (c) T. Sakakura, J. Choi and H. Yasuda, *Chem. Rev.* 2007, **107**, 2365-2387.
8. (a) Y. Zhou, S. S. Hu, X. Ma, S. Liang, T. Jiang and B. Han, *J. Mol. Catal. A* 2008, **284**, 52-57. (b) A. A. G. Shaikh and S. Sivaram, *Chem. Rev.* 1996, **96**, 951-976.
9. (a) N. Sharma, S. S. Dhankhar, S. Kumar, T. J. D. Kumar and C. M. Nagaraja, *Chem. - Eur. J.* 2018, **24**, 16662-16669. (b) S. S. Dhankhar, N. Sharma, S. Kumar, T. J. D. Kumar and C. M. Nagaraja,

Chem. - Eur. J. 2017, **23**, 16204-16212. (c) K. R. Roshan, B. M. Kim, A. C. Kathalikkattil, J. Tharun, Y. S. Won and D. W. Park, *Chem. Commun.* 2014, **50**, 13664-13667. (d) K. R. Roshan, T. Jose, D. Kim, C. K. A. and D. W. Park, *Catal. Sci. Technol.* 2014, **4**, 963-970. (e) J. J. Sun, W. Cheng, Z. Yang, J. Wang, T. Xu, J. Xin and S. Zhang, *Green Chem.* 2014, **16**, 3071-3078. (f) C. M. Nagaraja, R. Haldar, T. K. Maji and C. N. R. Rao, *Cryst. Growth Des.* 2012, **12**, 975−981.

10. S. Soo Han and W. A. Goddard III, *J. Am. Chem. Soc.* 2007, **129**, 8422-8423.
11. (a) M. Higuchi, K. Nakamura, S. Horike, Y. Hijikata, N. Yanai, T. Fukushima, J. Kim, K. Kato, M. Takata, D. Watanabe, S. Oshima and S. Kitagawa, *Angew. Chem. Int. Ed.* 2012, **51**, 8369-8372. (b) K. L. Mulfort and J. T. Hupp, *J. Am. Chem. Soc.* 2007, **129**, 9604-9605.
12. (a) S. Staderini, G. Tuci, L. Luconi, P. Müller, S. Kaskel, A. Eychmüller, F. Eichler, G. Giambastiani and A. Rossin, *Eur. J. Inorg. Chem.* 2017, 4909–4918. (b) S. Staderini, G. Tuci, M. D'Angelantonio, F. Manoli, I. Manet, G. Giambastiani, M. Peruzzini and A. Rossin, *ChemistrySelect* 2016, **6**, 1123-1131. (c) A. Rossin, G. Tuci, G. Giambastiani and M. Peruzzini, *ChemPlusChem* 2012, **79**, 406-412.
13. J. Dong, Y. Huang, X. Qin, Y. Cheng, J. Hao, D. Wan, W. Li, X. Liu and J. You, *Chem. - Eur. J.* 2012, **18**, 6158-6162.
14. The $^{13}C\{^{1}H\}$ NMR assignment for the tertiary C atom (C4) of the thiazole ring has been made through a 2D ^{1}H-^{13}C HETCOR experiment.
15. M. J. Katz, Z. J. Brown, Y. J. Colón, P. W. Siu, K. A. Scheidt, R. Q. Snurr, J. T. Hupp and O. K. Farha, *Chem. Commun.* 2013, 9449-9451
16. H. M. Rietveld, *J. Appl. Cryst.* 1969, **2**, 65-71.
17. M. Yoon and D. Moon, *Microp. Mesop. Mater.* 2015, **215**, 116-122.
18. J. Rouquerol, P. Llewellyn and F. Rouquerol, in *Studies in Surface Science and Catalysis*, eds. P. L. Llewellyn, F. Rodriquez-Reinoso, J. Rouquerol and N. Seaton, Elsevier Amsterdam, 2007, vol. 160, p. 49.
19. N. Saeidi and M. Parvin, *Periodica Polytech., Chem. Eng.* 2016, **60**, 123-129.

20. (a) X. Zhu, C. Tian, G. M. Veith, C. W. Abney, J. Dehaudt and S. Dai, *J. Am. Chem. Soc.* 2016, **138**, 11497–11500. (b) X. Zhu, S. M. Mahurin, S.-H. An, C.-L. Do-Thanh, C. Tian, Y. Li, L. W. Gill, E. W. Hagaman, Z. Bian, J.-H. Zhou, J. Hu, H. Liu and S. Dai, *Chem. Commun.* 2014, **50**, 7933-7936.
21. J. Schell, N. Casas, R. Pini and M. Mazzotti, *Adsorption* 2012, **18**, 49-65.
22. C. M. Simon, B. Smit and M. Haranczyk, *Comput. Phys. Commun.* 2016, **200**, 364–380.
23. (a) Y. J. Colon, D. A. Gomez-Gualdron and R. Q. Snurr, *Cryst. Growth Des.* 2017, **17**, 5801-5810. (b) D. A. Gómez-Gualdrón, Y. J. Colón, X. Zhang, T. C. Wang, Y. Chen, J. T. Hupp, T. Yildirim, O. K. Farha, J. Zhang and R. Q. Snurr, *Energy Environ. Sci.* 2016, **9**, 3279-3289.
24. E. Argueta, J. Shaji, A. Gopalan, P. Liao, R. Q. Snurr and D. A. Gómez-Gualdrón, *J. Chem. Theory Comput.* 2018, **14**, 365-376.
25. C. M. Breneman and K. B. Wiberg, *J. Comput. Chem.* 1990, **11**, 361-373
26. M. J. Frisch, G. W. Trucks, H. B. Schlegel, G. E. Scuseria, M. A. Robb, J. R. Cheeseman, G. Scalmani, V. Barone, G. A. Petersson, H. Nakatsuji, X. Li, M. Caricato, A. V. Marenich, J. Bloino, B. G. Janesko, R. Gomperts, B. Mennucci, H. P. Hratchian, J. V. Ortiz, A. F. Izmaylov, J. L. Sonnenberg, Williams, F. Ding, F. Lipparini, F. Egidi, J. Goings, B. Peng, A. Petrone, T. Henderson, D. Ranasinghe, V. G. Zakrzewski, J. Gao, N. Rega, G. Zheng, W. Liang, M. Hada, M. Ehara, K. Toyota, R. Fukuda, J. Hasegawa, M. Ishida, T. Nakajima, Y. Honda, O. Kitao, H. Nakai, T. Vreven, K. Throssell, J. A. Montgomery Jr., J. E. Peralta, F. Ogliaro, M. J. Bearpark, J. J. Heyd, E. N. Brothers, K. N. Kudin, V. N. Staroverov, T. A. Keith, R. Kobayashi, J. Normand, K. Raghavachari, A. P. Rendell, J. C. Burant, S. S. Iyengar, J. Tomasi, M. Cossi, J. M. Millam, M. Klene, C. Adamo, R. Cammi, J. W. Ochterski, R. L. Martin, K. Morokuma, O. Farkas, J. B. Foresman and D. J. Fox, *Gaussian 16 Rev. A.03*, Wallingford, CT, 2016.
27. (a) A. D. Becke, *J. Chem. Phys.* 1998, **98**, 5648-5652. (b) C. Lee, W. Yang and R. G. Parr, *Phys. Rev. B* 1988, **37**, 785-789.
28. M. J. Frisch and J. A. Pople, *J. Chem. Phys.* 1984, **80**, 3265-3269.
29. T. H. Dunning Jr. and P. J. Hay, *Modern Theoretical Chemistry*, Plenum, New York, 1977.

30. J. Hu, Y. Liu, J. Liu, C. Gu and D. Wu, *Microp. Mesop. Mater.* 2018, **256**, 25-31.

31. V. A. Bolotov, K. A. Kovalenko, D. G. Samsonenko, X. Han, X. Zhang, G. L. Smith, L. J. McCormick, S. J. Teat, S. Yang, M. J. Lennox, A. Henley, E. Besley, V. P. Fedin, D. N. Dybtsev and M. Schröder, *Inorg. Chem.* 2018, **57**, 5074–5082.

32. *Materials Studio*, Accelrys Software Inc., San Diego, CA 92121, USA, 2001.

33. A. K. Rappe, C. J. Casewit, K. S. Colwell, W. A. Goddard III and W. M. Skiff, *J. Am. Chem. Soc.* 1992, **114**, 10024–10035.

34. D. Dubbeldam, S. Calero, D. E. Ellis and R. Q. Snurr, *Mol. Simul.* 2016, **42**, 81-101.

35. Y. G. Chung, D. A. Gómez-Gualdrón, P. Li, K. T. Leperi, P. Deria, H. Zhang, N. A. Vermeulen, J. F. Stoddart, F. You, J. T. Hupp, O. K. Farha and R. Q. Snurr, *Sci. Adv.* 2016, **2**, e1600909.

36. (a) J. J. Potoff and J. I. Siepmann, *AlChE J.* 2001, **47**, 1676-1682. (b) M. G. Martin and J. I. Siepmann, *J. Phys. Chem. B* 1998, **102**, 2569–2577.

37. (a) Y. J. Colón and R. Q. Snurr, *Chem. Soc. Rev.* 2014, 5735-5749. (b) C. E. Wilmer, M. Leaf, C. Y. Lee, O. K. Farha, B. G. Hauser, J. T. Hupp and R. Q. Snurr, *Nat. Chem.* 2012, **4**, 83–89.

38. P. Li, N. A. Vermeulen, C. D. Malliakas, D. A. Gómez-Gualdrón, A. J. Howarth, B. L. Mehdi, A. Dohnalkova, N. D. Browning, M. O'Keeffe and O. K. Farha, *Science* 2017, **356**, 624-627.

39. M. O'Keeffe, M. A. Peskov, S. J. Ramsden and O. M. Yaghi, *Acc. Chem. Res.* 2008, **41**, 1782-1789. http://rcsr.anu.edu.au/

40. J. H. Cavka, S. Jakobsen, U. Olsbye, N. Guillou, C. Lamberti, S. Bordiga and K. P. Lillerud, *J. Am. Chem. Soc.* 2008, **130**, 13850-13851.

41. M. Kim and S. M. Cohen, *CrystEngComm* 2012, **14**, 4096–4104.

42. R. J. Marshall, C. L. Hobday, C. F. Murphie, S. L. Griffin, C. A. Morrison, S. A. Moggach and R. S. Forgan, *J. Mater. Chem. A* 2016, **4**, 6955-6963.

43. C. V. McGuire and R. S. Forgan, *Chem. Commun.* 2015, **51**, 5199-5217.

44. M. Eddaoudi, J. Kim, N. Rosi, D. Vodak, J. Wachter, M. O'Keeffe and O. M. Yaghi, *Science* 2002, **295**, 469–472.

45. H. Furukawa, F. Gándara, Y.-B. Zhang, J. Jiang, W. L. Queen, M. R. Hudson and O. M. Yaghi, *J. Am. Chem. Soc.* 2014, **136**, 4369-4381.

46. O. V. Gutov, S. Molina, E. C. Escudero-Adán and A. Shafir, *Chem. - Eur. J.* 2016, **22**, 13582-13587.

47. H. Wang, Q. Wang, S. J. Teat, D. H. Olson and J. Li, *Cryst. Growth Des.* 2017, **17**, 2034-2040.

48. A. L. Spek, *Acta Crystallogr. Sect. D* 2009, **65**, 148–155.

49. (a) S. Yuan, Y.-P. Chen, J.-S. Qin, W. Lu, L. Zou, Q. Zhang, X. Wang, X. Sun and H.-C. Zhou, *J. Am. Chem. Soc.* 2016, **138**, 8912-8919. (b) C. L. Hobday, R. J. Marshall, C. F. Murphie, J. Sotelo, T. Richards, D. R. Allan, T. Duren, F.-X. Coudert, R. S. Forgan, C. A. Morrison, S. A. Moggach and T. D. Bennett, *Angew. Chem. Int. Ed.* 2016, **55**, 2401-2405. (c) F. Drache, V. Bon, I. Senkovska, M. Adam, A. Eychmuller and S. Kaskel, *Eur. J. Inorg. Chem.* 2016, 4483-4489. (d) C.-X. Chen, Z. Wei, J.-J. Jiang, Y.-Z. Fan, S.-P. Zheng, C.-C. Cao, Y.-H. Li, D. Fenske and C.-Y. Su, *Angew. Chem. Int. Ed.* 2016, **34**, 10086-10090. (e) S. Yuan, W. Lu, Y.-P. Chen, Q. Zhang, T.-F. Liu, D. Feng, X. Wang, J. Qin and H.-C. Zhou, *J. Am. Chem. Soc.* 2015, **137**, 3177-3180. (f) B. Wang, H. Huang, X.-L. Lv, Y. Xie, M. Li and J.-R. Li, *Inorg. Chem.* 2014, **53**, 9254-9259. (g) G. Nickerl, M. Leistner, S. Helten, V. Bon, I. Senkovska and S. Kaskel, *Inorg. Chem. Front.* 2014, **1**, 325-330.

50. V. A. Blatov, A. P. Shevchenko and D. M. Proserpio, *Cryst. Growth Des.* 2014, **14**, 3576-3586. http://topospro.com/

51. J. R. Anderson, H. Kleinke and H. F. Franzen, *J. Alloys Compd.* 1997, **259**, L14-L18.

52. Benzoic acid pKa = 4.20; thiophene-2-carboxylic acid pKa = 3.51. Thus, benzoate is a stronger base than thiophene-2-carboxylate and forms stronger coordinative bonds with Zirconium. Judging from the TG results reported here, thiazole-5-carboxylate basicity presumably lies in between that of benzoate and of thiophene-2-carboxylate (direct experimental data not available).

53. L. Ding, B. Yao, W. Jiang, J. Li, Q. Fu, Y. Li, Z. Liu, J. Ma and Y. Dong, *Inorg. Chem.* 2017, **56**, 2337-2344.

54. P. Xydias, I. Spanopoulos, E. Klontzas, G. E. Froudakis and P. N. Trikalitis, *Inorg. Chem.* 2014, **53**, 679−681.

55. N. Ko, J. Hong, S. Sung, K. E. Cordova, H. J. Park, J. K. Yang and J. Kim, *Dalton Trans.* 2015, **44**, 2047–2051.

56. T. F. Willems, C. H. Rycroft, M. Kazi, J. C. Meza and M. Haranczyk, *Microp. Mesop. Mater.* 2012, **149**, 134-141.

57. L. D. Gelb and K. E. Gubbins, *Langmuir* 1999, **15**, 305-308.

58. P. García-Holley, B. Schweitzer, T. Islamoglu, Y. Liu, L. Lin, S. Rodriguez, M. H. Weston, J. T. Hupp, D. A. Gómez-Gualdrón, T. Yildirim and O. K. Farha, *ACS Energy Lett.* 2018, **3**, 748-754.

59. W. Humphrey, A. Dalke and K. Schulten, *J. Molec. Graphics* 1996, **14**, 33-38.

60. (a) B. Ugale, S. Kumar, T. J. D. Kumar and C. M. Nagaraja, *Inorg. Chem.* 2019, **58**, 3925-3936. (b) J. F. Kurisingal, Y. Rachuri, R. S. Pillai, Y. Gu, Y. Choe and D.-W. Park, *ChemSusChem* 2019, **12**, 1033-1042.

61. (a) J. Zhu, P. M. Usov, W. Xu, P. J. Celis-Salazar, S. Lin, M. C. Kessinger, C. Landaverde-Alvarado, M. Cai, A. M. May, C. Slebodnick, D. Zhu, S. D. Senanayake and A. J. Morris, *J. Am. Chem. Soc.* 2018, **140**, 993−1003. (b) J. Li, Y. Ren, C. Yue, Y. Fan, C. Qi and H. Jiang, *ACS Appl. Mater. Interfaces* 2018, **10**, 36047−36057. (c) C.-Y. Gao, J. Ai, H.-R. Tian, W. D. and Z.-M. Sun, *Chem. Commun.* 2017, **53**, 1293-1296. (d) S. Demir, S. Usta, H. Tamar and M. Ulusoy, *Microp. Mesop. Mater.* 2017, **244**, 251-257. (e) S. Yuan, L. Zou, H. Li, Y.-P. Chen, J. Qin, Q. Zhang, W. Lu, M. B. Hall and H.-C. Zhou, *Angew. Chem. Int. Ed.* 2016, **55**, 10776 –10780.

62. (a) J. Liang, R.-P. Chen, X.-Y. Wang, T.-T. Liu, X.-S. Wang, Y.-B. Huang and R. Cao, *Chem. Sci.* 2017, **8**, 1570-1575. (b) L.-G. Ding, B.-Y. Yao, W.-L. Jiang, J.-T. Li, Q.-J. Fu, Y.-A. Li, Z.-H. Liu, J.-P. Ma and Y.-B. Dong, *Inorg. Chem.* 2017, **56**, 2337-2344.

63. R. Vismara, G. Tuci, N. Mosca, K. V. Domasevitch, C. Di Nicola, C. Pettinari, G. Giambastiani, S. Galli and A. Rossin, *Inorg. Chem. Front.* 2019, **6**, 533-545.

64. (a) B. Mousavi, S. Chaemchuen, B. Moosavi, K. Zhou, M. Yusubov and F. Verpoort, *ChemistryOpen* 2017, **6**, 674 – 680. (b) J. Tharun, K.-M. Bhin, R. Roshan, D. W. Kim, A. C. Kathalikkattil, R. Babu, H. Y. Ahn, Y. S. Won and D.-W. Park, *Green Chem.* 2016, **18**, 2479-2487. (c) Y.-H. Han, Z.-Y.

Zhou, C.-B. Tian and S.-W. Du, *Green Chem.* 2016, **18**, 4086-4091. (d) X. Huang, Y. Chen, Z. Lin, X. Ren, Y. Song, Z. Xu, X. Dong, X. Li, C. Hu and B. Wang, *Chem. Commun.* 2014, **50**, 2624-2627. (e) X. Zhou, Y. Zhang, X. Yang, L. Zhao and G. Wang, *J. Mol. Catal. A: Chem.* 2012, **361-362**, 12-16. (f) C. M. Miralda, E. E. Macias, M. Zhu, P. Ratnasamy and M. A. Carreon, *ACS Catal.* 2012, **2**, 180-183.

Table of Contents Entry

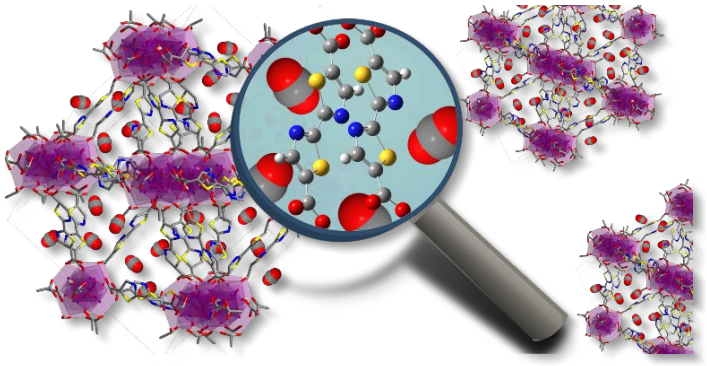

A combined theoretical-experimental approach has been exploited for the design of a zirconium bithiazole-based MOF for CO_2 adsorption and its reaction with epoxides under green conditions.